

Active percolation analysis of pyramidal neurons of somatosensory cortex: A comparison of wildtype and p21H-ras^{Val12} transgenic mice

Luciano da Fontoura Costa and Marconi Soares Barbosa

Instituto de Física de So Carlos

Universidade de So Paulo Caixa Postal 369 CEP 13560.970 So Carlos, SP, Brazil

e-mail: marconi@if.sc.usp.br

Andreas Schierwagen

Institute for Computer Science

University of Leipzig, D-04109 Leipzig, Germany

Alán Alpár and Ulrich Gärtner and Thomas Arendt

Department of Neuroanatomy

Paul Flechsig Institut for Brain Research, University of Leipzig, D-04109 Leipzig, Germany

Abstract

This article describes the investigation of morphological variations among two set of neuronal cells, namely a control group of wild type rat cells and a group of cells of a transgenic line. Special attention is given to singular points in the neuronal structure, namely the branching points and extremities of the dendritic processes. The characterization of the spatial distribution of such points is obtained by using a recently reported morphological technique based on forced percolation and window-size compensation, which is particularly suited to the analysis of scattered points presenting several coexisting densities. Different dispersions were identified in our statistical analysis, suggesting that the transgenic line of neurons is characterized by a more pronounced morphological variation. A classification scheme based on a canonical discriminant function was also considered in order to identify the morphological differences.

1 Introduction

During brain development, neurons form complex dendritic and axonal arbors that reach a characteristic pattern and size [1]. The development of arbor shape is partly determined by genetic factors and partly by interactions with the surrounding tissue (e.g. [2, 3, 4]). Dendritic growth is known to be responsive to various environmental signals, including synaptic activity and guidance molecules [5, 3, 6]. The impact of neurotrophins upon cortical neurons has gained special interest, since they are essential for neuronal development, as well as for the maintenance of functional stability and plasticity in the adult nervous system [7, 8, 9, 10].

Both neuronal activity and neurotrophins guide dendritic development via GTPase-dependent mechanisms [5, 11, 12]. Recent studies have drawn attention onto the small G-protein p21Ras in dendritic growth [13, 14, 15]. Like other GTPases, p21Ras regulates the phosphorylation of downstream kinases which trigger cascade mechanisms resulting in the regulation of enzymatic activities, ionic channels, cellular morphology and gene expression [16, 17, 18].

Effects of p21Ras have been shown to be essential for the normal functioning and plasticity of both the developing [19, 20, 21] and the adult nervous systems [22, 23, 24]. Furthermore, enhanced expression of p21Ras is associated with neuronal restructuring after lesion or in the context of neurodegenerative diseases [25, 26, 27].

investigated in p21H-Ras^{Val12} transgenic mice [28, 13, 14]. In this model the expression of transgenic p21H-Ras^{Val12} starts postnatally around day 15, when neurons are postmitotic and the majority of synaptic contacts has been established. In particular cortical pyramidal neurons express the transgenic construct at high levels. The volume of the cerebral cortex of these transgenic mice is increased by approximately 20% compared to wildtype mice. This increase has been attributed to the enlarged volume of the cortical pyramidal cells, but not to a raise in the number of neurons [29, 28, 13, 14].

Dendritic morphology of pyramidal cells is very heterogeneous, not only in different areas (e.g. [30]) but also within the same region (e.g. [31]). To set the population of neurons for investigation, only commissural neurons of layers II/III of the primary somatosensory cortex have been analysed in this study. By means of this restriction the analysis of a relatively homogeneous subpopulation of pyramidal neurons became possible.

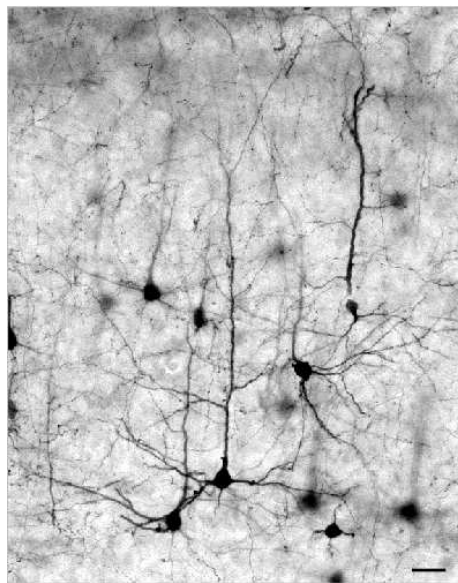


Figure 1: Retrogradely pyramidal neurons in layers II/III of the primary somatosensory cortex. Scale bar: $50\mu m$.

In a previous study we found that enhanced p21Ras activity results in a dramatically enlarged dendritic tree. In both cortical layers II/III and V, the total surface area and the total volume of dendritic trees is greatly increased. This is mainly caused by increased dendritic diameter and by the appearance of additional segments [32].

On the other hand, topological complexity of pyramidal neurons in layers II/III appeared hardly affected: Sholl analysis of both basal and apical dendrites revealed no differences between transgenic and wildtype mice regarding any parameters considered, i.e. numbers of intersections, branching points and tips [32].

These results suggest a rather proportional increase of dendritic tree size, without distinct changes in the space-filling properties. The aim of the present study was to substantiate these findings.

In the present work we consider the use of a new procedure, known as percolation transform [33, 34], which is particularly useful for characterization of spatial density of distributed points. This framework represents an enhanced alternative to the multiscale fractal analysis reported before [35]. The percolation transform procedure consists of two steps. The first is to induce an active percolation dynamics by performing an exact dilation of the points. During this process, the number of mergings between points and connected groups of points is recorded for each dilation radius. Having recorded the accumulative number of mergings as a function of scale, an essential normalization procedure is performed in order to compensate for sparser distributions which would have produced a much weaker signal otherwise.

The overall enhanced sensitivity is a direct consequence of recording only mergings or shocks between

increase in area as considered in the (multiscale) fractal analysis [35]. This enhanced type of analysis is particularly suitable in the present case because the percolation transform approach is independent of size-related parameters like area and volume of the neuronal cells. We argue that changes in the global character of the percolation transform curves, derived from the reference points (i.e. dendrite extremities and branch points) of the dendrites of pyramidal neurons due to transgenic activation of p21Ras in the primary somatosensory cortex of mice, correlate with changes in the complexity of neuronal morphology.

2 Materials and methods

2.1 Biological

We used data derived from experiments with three transgenic mice aged nine months (see [29, 28] for the establishment of the transgenic mouse line), as well as with three wildtype mice of the same age. All experimental procedures on animals were carried out in accordance with the European Council Directive of 24 November 1986 (86/609/EEC) and had been approved by the local authorities. All efforts were made to minimise the number of animals used and their suffering.

Mice were anaesthetised with Hypnomidate[®] (Janssen-Cilag) (1ml/40g body weight intraperitoneally) and positioned in a stereotaxic apparatus. Prior to incision 0.1ml Xylonest[®] (Astra) was injected below the skin, the left parietal bone was partially removed, Using a Hamilton syringe for unilateral injection, Biotinylated Dextran Amine (11 20% BDA, 10.000 nominal molecular weight(MW), Molecular Probes) was mechanically delivered into the corpus callosum 1mm lateral to the midline and 0.5 mm caudal to the bregma, 1mm deep from pial surface according to the stereotaxic atlas of Frankin and Paxinos (1997). Seven days after surgery the animals were intracardially perfused in deep anaesthesia, first with saline (0.9% NaCl) for 1-2 min and then with a fixative containing 4% paraformaldehyde in 0.1 M phosphate buffer (pH 7.4) for 30 min. The brains were postfixed in the same solution overnight, immersed in 30% sucrose for another 24 hours, and sectioned (160 μ m) in the coronal plane on a cryostat. The free-floating sections were extensively washed in 0.05 M Tris Buffered Saline (TBS, pH 7.4), and then reacted with the avidin-biotin-peroxidase complex (1:100 in TBS, VECTASTAIN[®] Elite ABC kit, Vector Laboratories, Inc.) at room temperature for two hours. BDA was visualised by using 3,3-diamino-benzidine (Sigma, 0.025%) intensified with nickel-ammonium sulphate (Merck, 0.05%) in the presence of 0.001% hydrogen peroxide, diluted in TBS. Sections were mounted onto gelatine coated glass slides, dehydrated and covered with DPX (Fluka, Neu-Ulm, Germany).

The retrogradely labelled pyramidal cells were reconstructed using NeuroLucida[®] (MicroBrightField, Inc.), see Figure 1. The system allowed accurate tracing of the cell processes in all three dimensions and continuous adjustment of the dendritic diameter with a circular cursor. A motorized stage with position encoders enabled the navigation through the section in the xyz axes and the accurate acquisition of the spatial coordinates of the measured structure. All visible dendrites were traced without marking eventual truncation of smaller dendritic sections. This may have led to certain underestimation of the dendritic tree, especially in transgenic mice with a larger dendritic arbour. To gain both optimal transparency for optimal tracing facilitates and at the same time a possibly complete neuronal reconstruction, sections of 160 μ m thickness were used. Thicker sections allowed only ambiguous tracing of thinner dendritic branches. Shrinkage correction (300%) was carried out in the z axis, but not in the xy plane, because shrinkage was negligible in these dimensions (10%).

The morphology files created by NeuroLucida[®] need to be edited and converted to a simpler file format before they can be used for further analyses. We used for this purpose the freely available program Cvapp [36]. Cvapp is a cell viewing, editing and format converting program for morphology files, see Figure 2. It can be also used to prepare structures digitized with NeuroLucida[®] software for modeling with simulators like

to the SWC format describing the structure of a neuron in the simplest possible way [37].

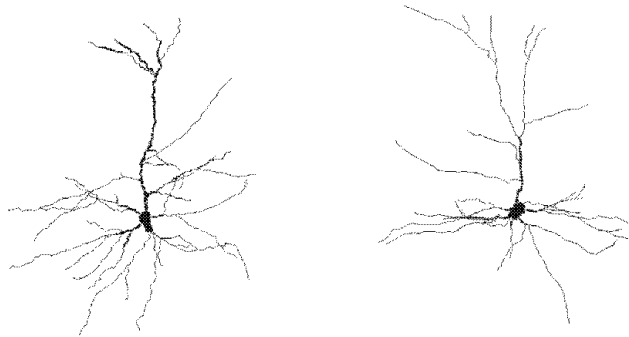


Figure 2: Pyramidal cells rendered with Cvapp. Displayed are random examples of each transgenic neuron (cell SE8, left) and wildtype neuron (cell WT19, right).

Each line encodes the properties of a single neuronal compartment. The format of a line in a SWC file is as follows: $n \ T \ x \ y \ z \ R \ P$. In turn, these numbers mean: (1) an integer label (normally increasing by one from one line to the next) that identifies the compartment, (2) an integer that represents the type of neuronal segment (0-undefined, 1-soma, 2-axon, 3-dendrite, 4-apical dendrite, etc.) , (3)-(5) xyz coordinate of compartment , (6) radius of compartment, (7) parent compartment (defined as -1 for the initial compartment). The sample of neurons edited, converted and analyzed (see below) comprised 28 of wildtype neurons and 26 of transgenic neurons.

2.2 Computational

The concept of the percolation transform [33, 34] is described in the following. As mentioned in Section 1 this method uses of a mechanism known as Minkowski dilation. Given a set of points S in R^3 , its Minkowski dilation by a radius r corresponds to the union of closed balls of radius r_i placed over each point in S , and the volume of the dilated set is represented as $V(r_i)$. In order to ensure enhanced precision and computational efficiency, only those radiuses corresponding to the viable distances in the orthogonal lattice, the so-called exact distances [38], are taken into account.

Consider now that the set of points S is generated from a Poisson distribution with density γ inside a cubic window of side L . Let $C(d_i)$ be a function that counts the number of mergings between growing clusters at a specific distance $d_i = 2r_i$ as the whole set of points undergoes a dilation by radius r_i . In order to allow scale uniformity we make the change of variables $k_i = \ln(d_i)$. A graphic representation of this function is shown in Figure 3 for two different values of density γ_1 and γ_2 . One can see that there is a characteristic scale for each density, where most of the merging dynamics takes place before reaching a plateau. The total number of points in S is given by $\gamma_1 V$ or $\gamma_2 V$ as illustrated by Figure 3. The idealized scenario where this dynamics occurs is represented by the unit step functions. In our model, the position of such a transition is taken as the characteristic scale for the set S .

Next, we need to relate the characteristic scales to the densities of the generated Poisson set of points. We argue that the distance where all points suddenly collapse into a unique cluster is in fact the mean nearest neighbor distance. Knowing the nearest neighbor distance distribution [39] for the three-dimensional space, the mean nearest neighbor distance as a function of the density of the cloud can be expressed as

$$\bar{d} = \frac{0.554}{\sqrt[3]{\gamma}}. \quad (1)$$

The smooth curve represents the behaviour of the shock dynamics for a Poisson model, while the unnormalized Dirac deltas stands for the idealized model. Note that the rate of change of the cumulative number of mergings for higher scales tends to decrease fastly. As we intend to use these characteristic scales to detect multiple densities coexisting in the same set of points, we need a normalization procedure in order to enhance the signal for sparser distributions of points, therefore assigning the same importance to all scales. To implement such a normalization we take as reference the maximum value of the rate of change for one specific reference scale k_j . The function we need should always give the same value irrespectively of the characteristic scale we are dealing with, as in the following equation

$$Q(\bar{k}_i) = \frac{P(\bar{k}_i)}{\Delta \bar{k}_j} e^{(3\bar{k}_i - 3\bar{k}_j)}. \quad (2)$$

This normalization procedure is the last step in the percolation approach. In the case of an experimental cumulative function obtained from a Poisson simulation with specific density, Equation 2 will produce the same intensity for any density value. When dealing with an experimental cumulative function involving an unknow mixture of densities, Equation 2 will yield detect the multiple characteristic distances actually occurring in the sampled space.

We illustrate the potential of this procedure regarding coexisting densities of spatially distributed points for the following experimental example. Figure 5 presents an example pattern (inset) and the corresponding percolation transform curve. The example pattern consists of two Poisson clouds with distinct densities. The percolation curve for this example shows clearly the two peaks corresponding to the characteristics scales associated with the two different densities. Note that the difference in height of those peaks reflects the relative area occupied by each cloud.

In the present work we consider the spatial distribution of the singular points of the dendritic trees, i.e. dendritic branch points and extremities. Such an approach (see [40, 41]) has shown to be an effective route when dealing with subtle geometrical changes while considering a single morphological/physiological class of neuronal cells.

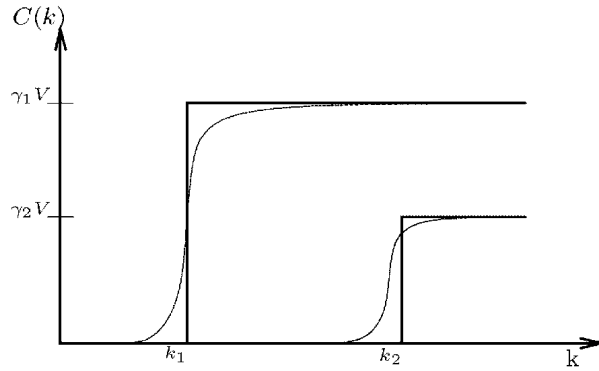


Figure 3: The smooth curve shown corresponds (schematically) to the accumulative mergings as a function of the characteristic scale for a Poisson distribution of points. The unit-step functions shown come from idealized assumptions.

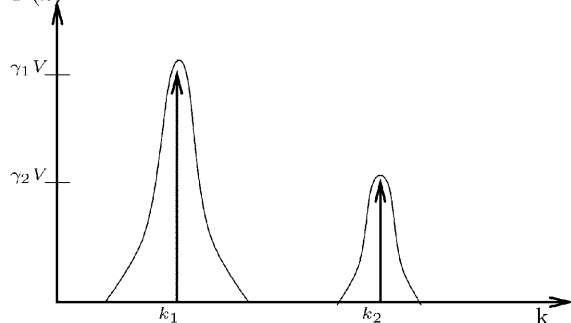


Figure 4: The derivative of the cumulative merging function, as a function of the characteristic scale. Schematically as before the smooth curves stands for Poisson clouds and the Kronecker functions, represented as upward arrows, are associated with the idealized model.

3 Results

Figure 6 shows the resulting percolation transform curve for the two selected cells of Figure 2. The overall profile of these curves were the same, showing two proeminent peaks at clearly distinguishable scales ¹. Although we can see that these two single cells presents a clearly distinc global features in their signature curve, this property is masked by the statistical variabilities of the whole set of cells, as shown by the scatter plot in Figure 7. This scatter plot is an example of various quantile-quantile graphs we produced using global properties of all percolation curves, such as those exemplified in Figure 6. For this purpose, we select a few global properties, namely the mean, the variance, the maximum value, the scale at which the maximum value occur and the monotonicity index[42]. The scatterplot of Figure 7 is defined by the monotonicity index and the maximun scale, as an example of the overall variability of shapes. Taken pairwise none of these global measures leads to clear separation of the two types of cell involved in this study.

Before ruling out the possible existence of a geometrical characteristic that may be correlated with the genetic treatment, we performed a more thorough statistical analysis of the data produced by the percolation approach. These consist of a principal component analysis and a cononical discriminant analysis [43]. Figure 8 shows the density profile for the principal component variable, showing a similar mean but a pronouced difference in dispersion of the considered geometrical features of the genetically treated cells. Table 1 shows the performance of the those selected global features in providing a discriminant function for the two type of cells. While there is visible potential for classfyng one type of cells, namely the SE group, the discriminant function has a marginal performance concernig the other group, misclassifying almost half of them. This can be graphically visualized in Figure 9.

	SE	WT	Error	Posterior.Error
SE	20	7	0.2592593	0.3891051
WT	9	12	0.4285714	0.4767072
Overall			0.6878307	0.4274310

Table 1: The result of classical discriminant analysis for the measures considered in the scatterplot of Figure 7. From this cross-validation table we observe a somewhat better classifacation rate for type SE while for WT the estimation is indecisive.

¹Note that the scale axis is the logarithm of the actual distance among the points.

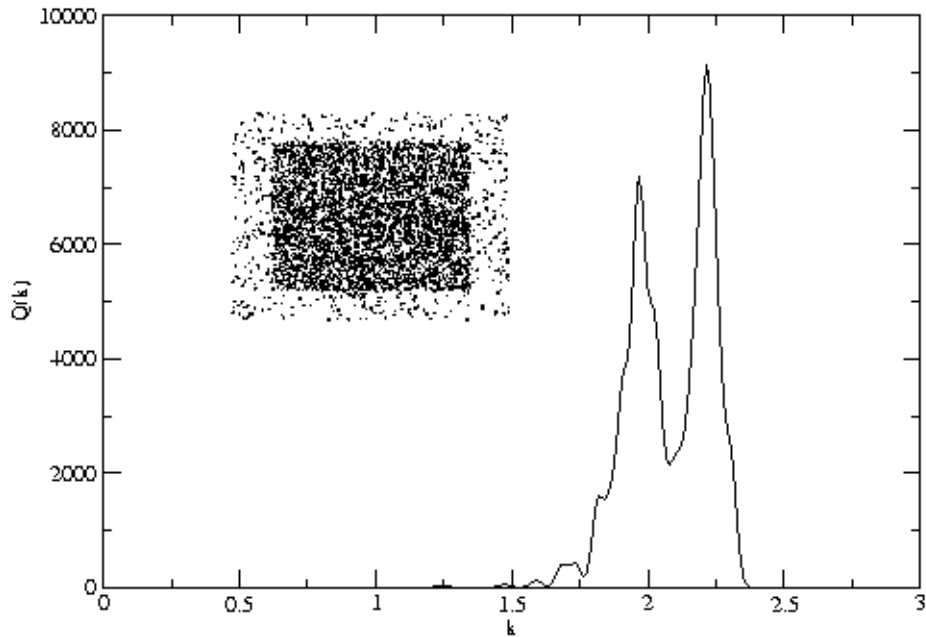


Figure 5: An example showing the resolving ability of the proposed procedure for the pattern show at the inset. The two coexisting densities are clearly detected by the peaks occurring at their characteristic scales.

4 Discussion

The present study is one of the few which uses 3D data on neuronal morphology to quantitatively characterize the complexity and scaling properties of different neuron types. The morphology of pyramidal cells was investigated in two sets of neurons, i.e. wildtype and p21H-rasVal12 transgenic mice. The results obtained using principal component analysis indicates that the transgenic neurons have a greater dispersion, as revealed by the density profiles shown in Figure 8. This finding may suggest that the enhanced p21Ras activity in transgenic mice may lead to greater variety of the cell morphological phenotype.

These results must be valuated with care, however. We know from other studies (e.g . Fernandez et al. 1994) that a measure like fractal dimension for example is not sufficient to differentiate between cell classes. Alone it does not completely specify a cells morphology but increases classification accuracy as an additional parameter for morphological classification among several other parameters typically used for placing nerve cells in different classes such as soma diameter, maximum dendritic diameter, number of branches etc. The same situation may have ocured here with the percolation transform approach. Although our findings suggest that transgenic mice pyramidal neurons exhibit a more variable dendritic morphology than the corresponding wild type neurons, this problem must be investigated in more detail. Clearly such study will include a more extended statistical analyses of the neuronal morphometrical parameters.

5 Acknowledgments

This study was partly supported by the Deutsche Forschungsgemeinschaft (grant GA716/1-1), FAPESP and CNPq.

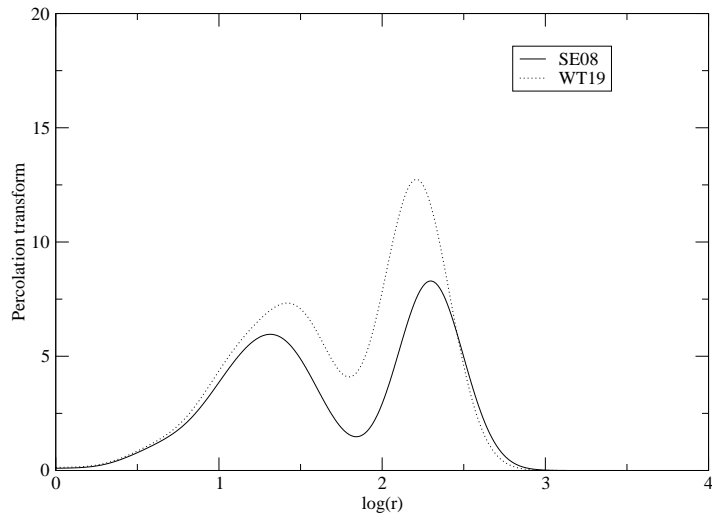


Figure 6: Example of the percolation curve for the two types of neuronal cells presented in Figure 2.

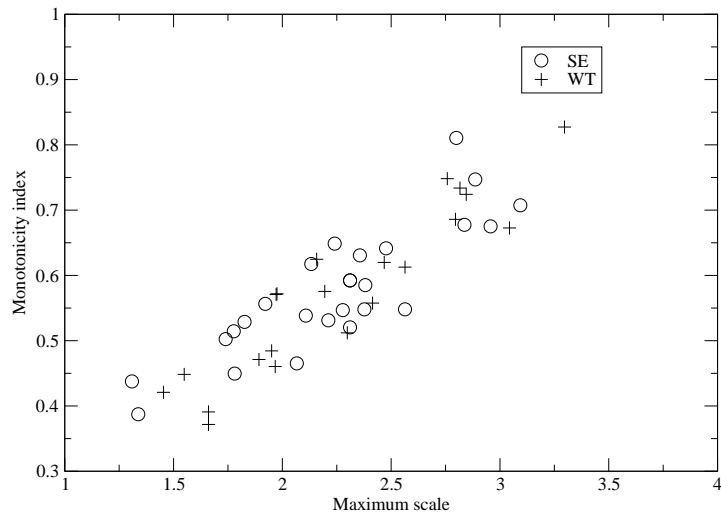


Figure 7: A scatter plot defined by the monotonicity index (vertical axis) and the scale (horizontal axis) at which the maximum of the percolation transform curve occurs.

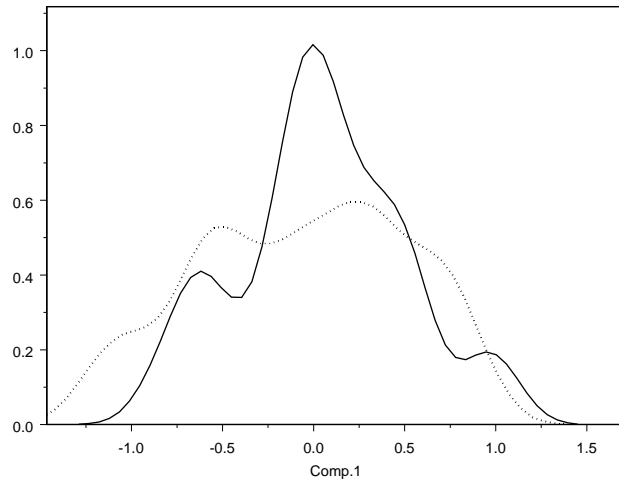


Figure 8: The density profile of the principal component score for each class in this experiment. One can see a very similar mean and broader dispersion in the WT cells shown by the dotted line.

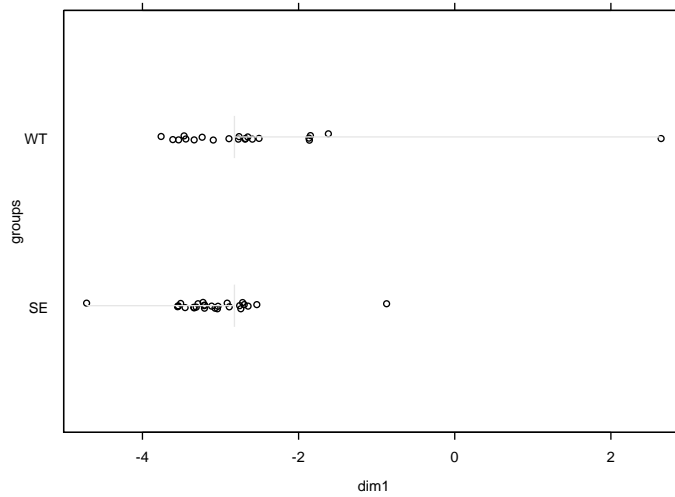


Figure 9: The graphical result of canonical analysis, showing the amount of discrimination possible for both classes of neurons with the one dimensional variable.

- [1] M. L. Feldman. Morphology of the neocortical pyramidal neuron. In E. G. Jones A. Peters, editor, *Cellular Components of the Cerebral Cortex*, volume 1, pages 123–200. Plenum Press, New York, 1984.
- [2] F. D. Miller and D. R. Kaplan. Signaling mechanisms underlying dendrite formation. *Curr. Opin. Neurobiol.*, 13:391–398, 2003.
- [3] E. K. Scott and L. Luo. How do dendrites take their shape? *Nat. Neurosci.*, 4:359–365, 2001.
- [4] R. O. Wong and A. Ghosh. Activity-dependent regulation of dendritic growth and patterning. *Nat. Rev. Neurosci.*, 3:803–812, 2002.
- [5] A. K. McAllister. Cellular and molecular mechanisms of dendrite growth. *Cereb Cortex*, 10:963–973, 2000.
- [6] K. L. Whitford, P. Dijkhuizen, F. Polleux, and A. Ghosh. Molecular control of cortical dendrite development. *Annu Rev Neurosci*, 25:127–149, 2002.
- [7] H. Thoenen. Neurotrophins and neuronal plasticity. *Science*, 270:593–598, 1995.
- [8] A. M. Davies. Neurotrophins: neurotrophic modulation of neurite growth. *Curr. Biol.*, 10:R198–200, 2000.
- [9] E. J. Huang and L. F. Reichardt. Neurotrophins: roles in neuronal development and function. *Annu. Rev. Neurosci.*, 24:677–736, 2001.
- [10] A. K. Allister. Neurotrophins and cortical development. *Results Probl. Cell Differ*, 39:89–112, 2002.
- [11] Z. Li, C. D. Aizenman, and H. T. Cline. Regulation of the rho gtpases by crosstalk and neuronal activity in vivo. *Neuron*, 33:741–750, 2002.
- [12] W. C. Sin, K. Haas, E. S. Ruthazer, and H. T. Cline. Dendrite growth increased by visual activity requires nmda receptor and rho gtpases. *Nature*, 419:475–480, 2002.
- [13] M. Holzer, U. Gärtner, F. J. Klinz, F. Narz, R. Heumann, and T. Arendt. Activation of mitogen-activated protein kinase cascade and phosphorylation of cytoskeletal proteins after neurone-specific activation of p21ras. i. mitogen-activated protein kinase cascade. *Neurosci.*, 105:1031–1040, 2001.
- [14] M. Holzer, L. Rödel, G. Seeger, U. Gärtner, F. Narz, C. Janke, R. Heumann, and T. Arendt. Activation of mitogen-activated protein kinase cascade and phosphorylation of cytoskeletal proteins after neurone-specific activation of p21ras. ii. cytoskeletal proteins and dendritic morphology. *Neurosci.*, 105:1041–1054, 2001.
- [15] E. J. Huang and L. F. Reichardt. Trk receptors: Roles in neuronal signal transduction. *Annu. Rev. Biochem.*, 72:609–642, 2003.
- [16] N. G. Ahn. The map kinase cascade. discovery of a new signal transduction pathway. *Mol. Cell Biochem.*, 127:201–209, 1993.
- [17] E. Nishida and Y. Gotoh. The map kinase cascade is essential for the diverse signal transduction pathways. *Trends Biochem. Sci.*, 18:128–131, 1993.
- [18] R. Heumann. Neurotrophin signalling. *Curr. Opin. Neurobiol.*, 4:668–679, 1994.
- [19] M. Noda, M. Ko, A. Ogura, D. G. Liu, T. Amano, T. Takano, and Y. Ikawa. Sarcoma viruses carrying ras oncogenes induce differentiation-associated properties in a neural cell line. *Nature*, 318:73–75, 1985.

morphological differentiation. *Cell*, 42:841–848, 1985.

- [21] I. Guerrero, H. Wong, A. Pellicier, and D. E. Burstein. Activated n-ras gene induces neuronal differentiation of pc12 rat pheochromocytoma cells. *J. Cell Physiol.*, 129:71–76, 1986.
- [22] R. Brambilla, N. Gnesutta, L. Minichiello, G. White, A. J. Roylance, C. E. Herron, M. Ramsey, D. P. Wolfer, V. Cestari, and C. Rossi-Arnaud. A role for the ras signalling pathway in synaptic transmission and long-term memory. *Nature*, 390:281–286, 1997.
- [23] A. J. Silva, P. W. Frankland, Z. Marowitz, E. Friedman, G. Lazlo, D. Cioffi, T. Jacks, and R. Bourchouladze. A mouse model for the learning and memory deficits associated with neurofibromatosis type i. *Nat. Genet.*, 15:281–284, 1997.
- [24] B. D. Moore, J. M. Slopis, E. F. Jackson, A. E. De Winter, and N. E. Leeds. Brain volume in children with neurofibromatosis type 1: relation to neuropsychological status. *Neurology*, 54:914–940, 2000.
- [25] L. L. Phillips and E. T. Belardo. Increase of c-fos and ras oncoproteins in the denerved neuropil of the rat detate gyrus. *Neuroscience*, 58:503–514, 1994.
- [26] U. Gärtner, M. Holzer, and T. Arendt. Induction of p21ras in alzheimer pathology. *Neuroreport*, 6:1313–1316, 1995.
- [27] U. Gärtner, M. Holzer, and T. Arendt. Elevated expression of p21ras is an early event in alzheimer’s disease and precedes neurofibrillary degeneration. *Neuroscience*, 91:1–5, 1999.
- [28] R. Heumann, C. Goemans, D. Bartsch, K. Lingenhöhl, P. C. Waldmeier, B. Hengerer, P. R. Allegrini, K. Schellander, E. F. Wagner, T. Arendt, R. H. Kamdem, K. Obst-Pernberg, F. Narz, P. Wahle, and H. Berns. Constitutive activation of ras in neurons promotes hypertrophy and protects from lesion-induced degeneration. *J. Cell Biol.*, 151:1537–1548, 2000.
- [29] R. Heumann, F. Narz, Y. Algür, D. Bartsch, M. Hüser, F. J. Klinz, E. Wagner, H. Berns, K. Obst-Pernberg, and P. Wahle. Neuronal modulation of p21ras activity in transgenic animals: A master switch? *J. Brain Res.*, 37:585, 1996.
- [30] G. N. Elson and K. S. Rockland. The pyramidal cell of the sensorimotor cortex of the macaque monkey: phenotypic variation. *Cereb. Cortex*, 12:1071–1078, 2002.
- [31] H. Duan, S. L. Wearne, J. H. Morrison, and P. R. Hof. Quantitative analysis of the dendritic morphology of corticocortical projection neurons in the macaque monkey association cortex. *Neuroscience*, 114:349–359, 2002.
- [32] A. Alpár, K. Palm, A. Schierwagen, T. Arendt, and U. Gärtner. Expression of constitutively active p21h-rasval12 in postmitotic pyramidal neurons results in increased dendritic size and complexity. 2003. Submitted.
- [33] L. da F. Costa. Actively-induced percolation: an effective approach to multi-object systems characterization. *arXiv:cond-mat/04*, 2004.
- [34] L. da F. Costa. Biological sequence analysis through the one-dimensional percolation transform and its enhanced version. *Bioinformatics*, 2004.
- [35] L. da F Costa, E. T. M. Manoel, F. Faucereau, J. Chelly, J. van Pelt, and G. Ramakers. A shape analysis framework for neuromorphometry. *Network: Comput. Neural Syst.*, 13:283–310, 2002.

- [37] D. Jaeger. Directions on how to use cvapp to convert neurolocida v3 files to genesis 2.1 .p file format. <http://www.compneuro.org/CDROM/docs/fileconversion.html>.
- [38] L. da F. Costa. Multidimensional scale-space shape analysis. In *International Workshop on Synthetic-Natural Hybrid Coding and Three Dimensional Imaging*, pages 214–217, Santorini, Greece, 1999.
- [39] S. Torquato, B. Lu, and J. Rubinstein. Nearest-neighbour distribution function for systems of interacting particles. *J. Phys. A: Math. Gen.*, 23:103–107, 1990.
- [40] M. S. Barbosa, L. da F. Costa, and E. S. Bernardes. Neuromorphometric characterization with shape functionals. *Phys. Rev. E*, 67:061910, 2003.
- [41] D. A. Sholl. Dendritic organization in the neurons of the visual and motor cortices of the cat. *J. Anat.*, 87:387–406, 1953.
- [42] M. S. Barbosa, L. da F. Costa, et al. Characterizing neuromorphologic alterations with additive shape functionals. *Eur. Phys. J. B*, 37:109–115, 2003.
- [43] G. J. McLachlan. *Discriminant analysis and statistical pattern recognition*. Wiley, 1992.